JOURNAL OF PROPULSION AND POWER
Vol. 27, No. 3, May–June 2011

Blade-Mounted Single Dielectric Barrier Discharge Plasma Actuators in Turbine Cascade

Julia E. Stephens,* Thomas Corke,† and Scott Morris‡
University of Notre Dame, Notre Dame, Indiana 46556

DOI: 10.2514/1.B34046

An experiment was conducted in a linear cascade of Pratt and Whitney Pack-B turbine blades to simulate the flow in the tip-gap region of a low-pressure turbine blade row. The objective was to investigate the sensitivity of the tip-clearance flow to blade-mounted plasma actuators designed to improve the net pressure loss coefficient. Investigations were performed at inlet Reynolds numbers of 0.2×10^6 and 0.5×10^6, corresponding to inlet Mach numbers of 0.08 and 0.2 and exit Mach numbers of 0.13 and 0.3, respectively. The gap-to-chord ratio was 4%. The flow was documented using endwall static pressure measurements and downstream pressure measurements using a five-hole pitot probe. The plasma actuators were operated to excite periodic disturbances that could couple with instabilities associated with the separated shear layer or bulk flow jetting from under the blade-wall gap. At the lower Reynolds number, the unsteady excitation resulted in as much as a 15% increase in mass-averaged total pressure loss. However, at the higher Reynolds number, the opposite occurred with a maximum of a 12.6% decrease in the total pressure loss. Both occurred at an actuator disturbance frequency that suggested that the actuator excited an instability of the shear layer between the tip-clearance flow and the passage flow.

I. Introduction

OVER the past decade, there have been a number of approaches proposed [1] to control the internal flow in gas turbine engines that are aimed at improving engine efficiency. Many of these approaches have focused on the compressor and turbine stages.

In the turbine stage, the flow that passes through the clearance gap between the blades and the casing is a major source of efficiency loss. First, the flow through the gap is not completely turned by the blades and thus does not contribute to the energy extraction. Second, the flow that exits the tip-gap develops into a coherent vortical structure. This structure, known as the tip-leakage vortex, produces losses in total pressure as it mixes with the mainstream flow. The vortices can interact with downstream components in the flow path and lead to strong unsteady pressures that can cause material fatigue. Additionally, the tip-leakage vortex concentrates high-temperature gas that induces hot spots that can cause material erosion. As a result of its importance to engine performance, the behavior of the tip-clearance flow, both in the tip-gap region and as it develops downstream, has been studied extensively [2–10].

A variety of flow control techniques have been examined to reduce the losses associated with the tip-leakage vortex. These can be categorized as either passive or active techniques. The passive flow control techniques involve fixed modifications or additions to the blade or endwall. The active flow control techniques modify the flow by injecting or removing mass, momentum, or adding a body force. Active flow control techniques include blowing [11], cooling [12,13], and plasma actuators [14–17].

The tip-leakage vortex has been found to be extremely sensitive to the blade tip geometry. Bindon and Morphis [18] experimentally investigated three blade tip geometries: a flat square-edged tip, a flat tip with a circular radius added to the pressure-side edge, and a fully contoured tip on which a circular radius was added to both the pressure- and suction-side edges. They found that applying a circular radius to the pressure-side edge of the blade significantly reduced the internal gap loss. They attributed this to the elimination of a separation bubble that existed on the underside of the blade tip. However, this also resulted in an increase in the downstream mixing losses.

This high degree of sensitivity was further manifested in the difficulty that Bindon and Morphis [18] had in repeating results between two identical blades. They concluded that creating two identical blades was very difficult and that the detailed flow phenomena was highly sensitive to small changes in tip geometry. Ameri and Bunker [19] performed numerical and experimental heat transfer investigations on sharp- and round-edged blades. Their findings indicated that the tip-leakage vortex forms further upstream on sharp-edged blades. Additionally, their studies showed that heat transfer on radiused tips was higher than on flat-tip blades.

Noting the impact that blade tip geometry has on the tip-gap flow, Heyes et al. [20] investigated wake pressure losses for various geometries. These investigations included flat-tip blades of various-edged radii, partial suction-side squealer tips, and partial pressure-side squealer tips. They found that both of the partial squealer-tip configurations reduced the wake loss compared with the flat tip. The suction-side squealer tip was found to be the most beneficial of the two configurations. Key and Arts [21] performed an extensive investigation of flat-tip and squealer-tip geometries. These investigations also showed a reduction in wake loss when squealer tips were implemented.

Douville [22] performed experiments in a linear cascade of Pack-B blades that investigated the effect of Reynolds number, gap size, and tip geometry. Douville found that by varying the tip-gap size for the same blade, the squealer tip had a greater impact on the tip-leakage vortex when the tip-gap was smaller. Douville suggested that this was due to differences in thick and thin blade characteristics. In addition to passive flow control techniques, active techniques designed to reduce the effects of the tip-leakage vortex have also been a topic of interest [23]. Such active techniques could have potential advantages over passive techniques, such as squealer tips, by not concentrating hot gas in the blade tip-gap region [19]. In addition, if the passive techniques do not use protruding elements, they are not at risk of damage due to rub events.

The results presented in this paper focus on active tip-clearance flow control using single dielectric barrier discharge (SDBD) plasma actuators. The mechanisms for SDBD plasma actuators have been thoroughly investigated and reported on in the literature [24–27].

Received 14 June 2010; revision received 4 November 2010; accepted for publication 4 January 2011.

*Graduate Research Assistant, Institute for Flow Physics and Control. Member AIAA.
†Clark Chair Professor, Institute for Flow Physics and Control. Associate Fellow AIAA.
‡Associate Professor, Institute for Flow Physics and Control. Member AIAA.

These actuators have been shown to work in a number of applications, including flow separation control on airfoils at high angles of attack [28] and along the midspan of Pratt and Whitney Pack-B blades [29–31]. More information on dielectric barrier discharge plasma actuators, the scaling of the body force, and applied voltage can be found in two recent reviews by Corke et al. [26,27].

The challenges of applying flow control to the turbine stage are exacerbated by the hot, turbulent gas. Any approaches that trap hot gas will likely enhance erosion on the engine parts due to the turbulent mixing of these gases. Therefore, a successful flow control strategy will have to minimize the desired effect as well as be robust enough to withstand this harsh environment. The plasma actuator has that potential if sufficient flow authority can be reached.

Considering this, the objective of this work was to investigate the use of plasma actuators located on the tips of Pack-B blades in a linear cascade. These were designed to modify the flow through the tip-clearance region in a manner that would reduce the loss coefficient measured in the blade wake. The approach would not rely on providing a restriction to the flow through the gap that could increase heat transfer to the blade in real applications.

II. Test Facility

This research was performed in a linear cascade with a stationary endwall in the Hessert Laboratory at the University of Notre Dame. A scale drawing of the cascade section of the facility is shown in Fig. 1. It consists of three blades forming two passages. A tailboard on the lowest blade allowed for adjustments of periodicity. The blades are Pratt and Whitney Pack-B profiles [30]. The blades had a chord length c of 11.7 cm (4.61 in.), an axial chord length c_x of 10.2 cm (4.14 in.), a span of 10.5 cm (4 in.), and a solidity σ of 1.13. The stagger angle of the blades was 26.16 deg.

All three of the blades were cast from a two-part epoxy using a numerically machined mold. The outer two blades spanned the entire cascade width. The center blade was shorter in span and cantilevered from the inside sidewall. Plastic shim stock placed between the blade and inside sidewall was used to vary the gap between the blade tip and the outside side wall. Tip gaps of up to 5% of axial chord were possible. For this study, the gap-to-axial-chord ratio was set at 4%.

Two inlet flow conditions were examined for this study. One had an inlet Mach number of 0.08. The exit Mach number in this case was 0.13, and the axial chord Reynolds number based on inlet velocity was 0.2×10^6. The other condition had an inlet Mach number of 0.2, with an accompanying exit Mach number of 0.3, and a chord Reynolds number based on inlet velocity of 0.5×10^6. These speeds are higher than those seen in typical linear cascades while remaining incompressible.

The flowfield in the wake of the center blade was documented using a five-hole pitot probe that was mounted to a motorized traverse system. The coordinate system for these measurements is shown in the schematic in Fig. 2. The measurements surveyed 5.1 cm (2 in.) in the pitch y direction and 3.2 cm (1.25 in.) in the span z direction. The surveys were performed at a distance of one axial chord length downstream of the trailing edge of the center blade. The total pressure at each point was measured through the center port of the probe. Secondary velocity vectors were determined based on the pressures from all ports and using the calibration approach described by Bryer and Pankhurst [32]. The resulting velocity vectors were accurate to a magnitude of $\pm 3\%$ when yaw and pitch angles were limited to $\pm 25°$. The five-hole probe was used to determine the total pressure loss and the streamwise vorticity of coherent motions associated with the tip-clearance flowfield. A detailed description of the calibration for this experiment is described by Stephens [33].

In addition to the five-hole probe, 30 static pressure ports were located on the endwall under the tip of the center blade. The locations of these static pressure ports with relation to the center blade are shown in Fig. 3.

III. Data Analysis

The endwall static pressure measurements were referenced to the static and total pressures at the inlet to the cascade, P_{si} and P_{ti}, respectively, which were measured with a pitot static probe located at the entrance to the cascade. The endwall static pressure coefficient was then defined as

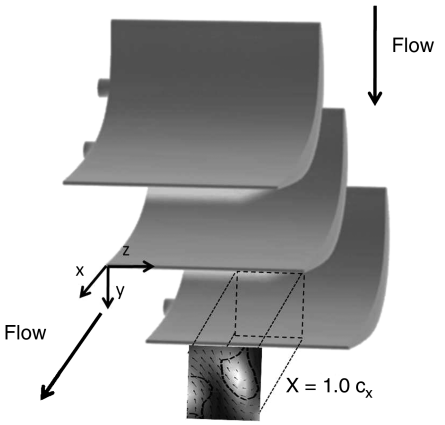

Fig. 2 Coordinate system for blade wake surveys made using five-hole pitot probe.

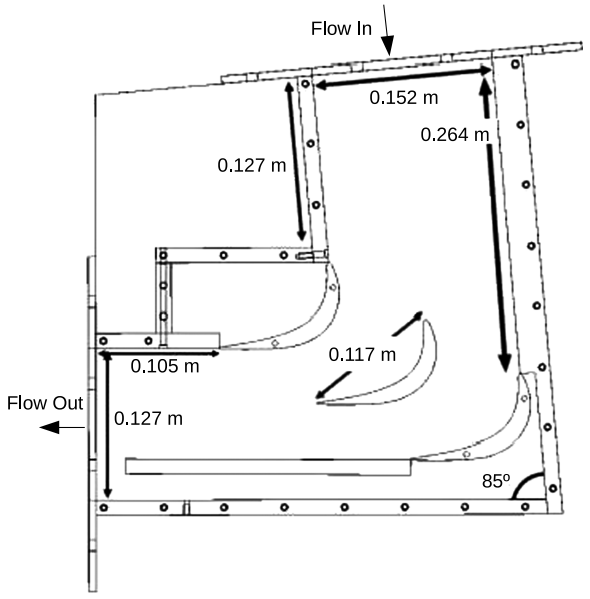

Fig. 1 Schematic drawing of transonic linear cascade facility.

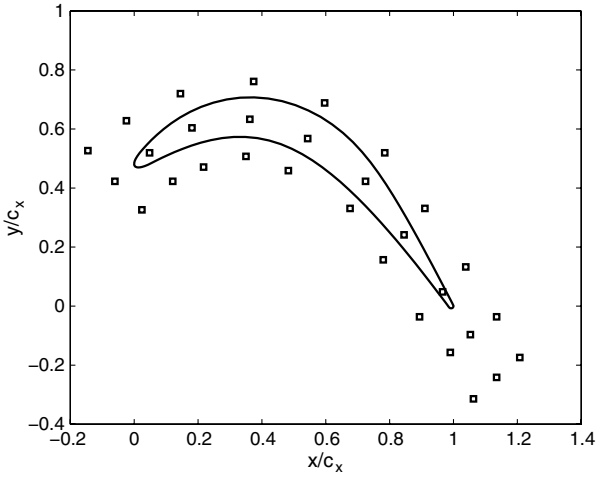

Fig. 3 Locations of static pressure ports on endwall.

$$c_p(k) = \frac{P_k - P_{si}}{P_{ti} - P_{si}} \tag{1}$$

where P_k is the static pressure at the kth location. All of the statistical averages of the pressure measurements were converged to within 1%.

The total pressure loss coefficient is related to the entropy production. Based on the five-hole probe measurements, the total pressure loss in the wake is

$$c_{pt} = \frac{P_{ti} - P_{te}}{P_{te} - P_{se}} \tag{2}$$

where P_{te} is the downstream total pressure measured by the center port of the five-hole probe, and P_{se} is a static pressure calculated using the other four ports of the five-hole probe.

The largest losses in the wake of the blade were assumed to be associated with coherent vortices such as the tip-leakage and passage vortices. Therefore, the $-\lambda_2$ method of Jeong and Hussain [34] was used to identify coherent vortices in the measurement region. This method identified vortices as regions bounded by contours of negative values of the second eigenvalue of the velocity gradient tensor. A closed constant level contour of a slightly negative eigenvalue is expected to enclose the outer boundary of a vortex. The lambda-2 criteria is a proven technique in the turbulent flow community that is derived from first principles. It was first introduced in 1995 and has since been used extensively in the analysis of computational fluid dynamics and experiment databases.

A combination of velocity vectors, total pressure loss contours, vorticity magnitude contours, and the $-\lambda_2$ contours were used to provide an indication of the locations and strengths of vortical structures that formed in the wake of the center blade in the cascade. A particular metric of merit used in evaluating the flow control was the loss coefficient C_{PT} associated with the tip-leakage vortex. To determine this, the pressure coefficients values c_{pt} that were inside regions bounded by zero-level λ_2 contours were mass averaged using the method of Yamamoto [2,3]. This formulation is given as

$$C_{PT} = \frac{\sum_k \sum_j (c_{pt} AU)_{k,j}}{\sum_k \sum_j (AU)_{k,j}} \tag{3}$$

where A is the area inside the zero-level λ_2 contour, and U is local velocity.

IV. Plasma Actuator

The general SDBD plasma actuator design consists of two electrodes separated by a dielectric layer, as is illustrated in Fig. 4. One electrode is exposed to the air (exposed electrode). The other electrode (covered electrode) is fully encapsulated by the dielectric layer. A high-voltage ac is supplied to the electrodes. When the ac voltage amplitude is large enough, the air over the covered electrode ionizes. The ionized air in the presence of the electric field produced by the electrode geometry results in a body force vector field that acts on the neutral air. The body force vector direction depends on the electrode geometry. In the arrangement in Fig. 4, the body force vector is directed toward the covered electrode. This results in a tangential wall jet of air. Reviews of SDBD plasma actuators have been given by Corke et al. [26,27,35].

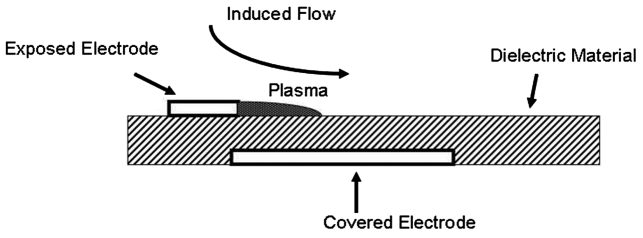

Fig. 4 General schematic of a SDBD plasma actuator with asymmetric electrodes.

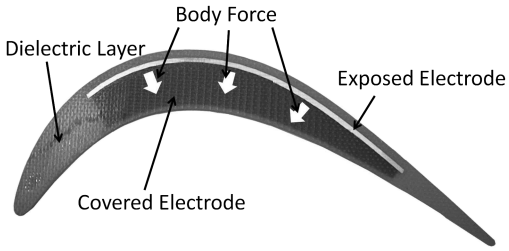

Fig. 5 Electrode configuration used for the blade-mounted plasma actuator.

For this research, a numerically controlled milling machine was used to fabricate a blade-mounted plasma actuator out of copper-clad glass-epoxy board. The epoxy board was milled on its edge to match the blade profile. The copper cladding was then milled off of both sides, leaving the covered and exposed electrodes. The exposed electrode was located along the suction-side edge in a configuration similar to a partial suction-side squealer tip. The covered electrode extended from that location toward the pressure side of the blade tip. This is shown in the photograph in Fig. 5. In the arrangement, the mean body force vector field opposes the flow that passes under the blade through the tip gap in such a way as to simulate the blockage achieved by a passive pressure-side squealer tip. The voltage used for the present research was 10 kV.

The plasma actuator design and operation are intended to produce a periodic disturbance that would excite a flow instability in the tip-gap region that could enhance mixing and alter the interaction between the tip-clearance and passage vortices. Figure 6 is a schematic of the tip-gap flowfield that illustrates two flow modules consisting of a two-dimensional (2-D) wall jet and a free shear layer. For simplification, a 2-D representation of the mean flow that passes thorough the gap between the blade tip and casing was considered. In reality, the mean flow through the gap has an axial component. Both of these flow modules are potentially unstable to disturbances. In each, there will be a dimensionless frequency that is most sensitive to excitation. This dimensionless frequency or Strouhal number β is given as

$$\beta = \frac{f \cdot l}{U} \tag{4}$$

where f is the dimensional instability frequency, l is a characteristic length scale, and U is a characteristic velocity. For free shear layers, a commonly used length scale is the momentum thickness. A representative velocity is the value at the edge of the shear layer. Typical Strouhal numbers of the most sensitive frequencies are on the order of $0.01 < \beta_s < 0.04$ [36]. For a viscous jet flow, a representative length scale is the diameter of the jet. The characteristic velocity is the velocity of the center of the jet. For circular jets, the most sensitive Strouhal numbers are typically $0.25 < \beta_j < 0.5$, but most often, $\beta_j = 0.44$ [36].

Bae et al. [23] investigated the instability of 2-D wall jets that were meant to simulate a blade tip-gap flow. They observed what appeared to be a preferred instability frequency when excited by unsteady synthetic jets at $\beta = 0.16$. This was then examined in a low-speed (6 m/s) low Reynolds number ($Re_c = 1 \times 10^5$) linear cascade, where it was observed to produce mixing enhancement. However, in

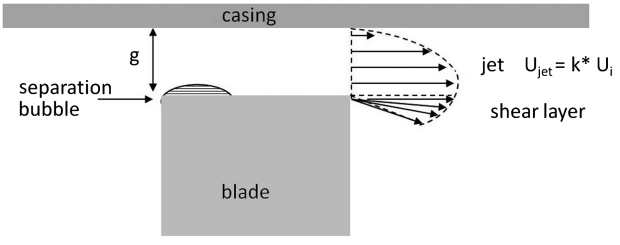

Fig. 6 Schematic of tip-gap flow with possible sources of flow instabilities.

that experiment, the net mass-averaged total pressure drop was not found to be affected.

With the plasma actuator, the ac frequency was on the order of 16 kHz, which was optimal for ionizing the air. A lower-frequency periodic disturbance was produced by switching the ac voltage on and off in a periodic manner. This method works as long as the portion of the period of the lower frequency when the actuator was on was sufficiently long enough to have at least two cycles of the higher-frequency ac. For this research, a duty cycle of 25% was used, resulting in an upper frequency limit of about 4 kHz.

V. Results

Surveying the entire wake region for a broad range of frequencies was infeasible for this study due to the time it takes to survey the window. As a first step to determine if the flow was sensitive to any particular frequencies, two locations in the wake were identified where the effect of the active flow control could be greatest. The choice of the locations of the discrete points was based on regions of large mean shear that would amplify even small changes that would signify a receptivity to the unsteady forcing. The metric of merit was a change in the mean flow that signified a change in the loss coefficient. One of these locations was inside the tip-leakage vortex, and the other was on the edge of the passage vortex. These locations are shown with respect to a spatial survey of the pressure loss coefficient for an inlet Reynolds number of 0.5×10^6 on the left side of Fig. 7. In the wake survey coordinates, the trailing edge of the blade is at the top edge of the plot and the endwall is along the right edge, as shown in Fig. 2. The velocity vectors were also determined from the five-hole probe. They give a sense of circulation in the two vortical structures. The tip-leakage vortex is on the right side of the spatial survey. The lighter contour at its center signifies that it contributes a large amount of total pressure loss, and the velocity vectors indicate the direction of circulation. The passage vortex is on the left side of the surveyed region. It has an opposite sense of circulation relative to the tip-leakage vortex. The loss coefficient associated with the passage vortex is less than that of the tip-leakage vortex. The dashed curves are the zero-level λ_2 contours. It is observed that these encircle the two coherent vortices and give an indication of their size.

The objective of the work was to find excitation frequencies that produced changes in the wake pressure distribution. Therefore, no distinction was made between changes that resulted in lower or higher loss coefficients. For this, the five-hole pitot probe was placed at one of the two spatial locations. The plasma actuator was operated, and the unsteady frequency was varied from 100 to 2100 Hz, corresponding to $0.01 \leq \beta \leq 0.12$. The absolute change in the pressure loss coefficient at the survey point was then recorded as a function of the excitation frequency. The results for the two survey locations at $Re = 0.5 \times 10^6$ are shown in the two plots on the right side of Fig. 7. The arrows from each plot point to the locations in the 2-D survey space where the point measurements were taken. The top plot corresponds to the measurement location in the approximate center of the tip-leakage vortex. The bottom plot corresponds to a location at the edge of the passage vortex. The approaching freestream speed and the tip-gap dimension were used as the characteristic velocity and length scale by which the frequencies were nondimensionalized to obtain the Strouhal number β.

For the spatial location inside the tip-leakage vortex, a large change in the total pressure occurred at $\beta \simeq 0.03$. For the spatial location at the edge of the passage vortex, a large change occurred for a $\beta \simeq 0.07$, which corresponds to a physical frequency of 1250 Hz. Measurements at this location were repeated, and this was the only frequency that gave a consistent large change.

If the observed peaks were due to a fluid instability, the dimensionless frequency should be constant. To check this, a similar experiment was performed at a lower inlet velocity corresponding to $Re_c = 0.2 \times 10^6$. The results for the same two relative measurement locations (centered in the tip-leakage vortex and at the edge of the passive vortex) are shown in Fig. 8. Again, for the location inside the tip-leakage vortex, a large change in the total pressure was observed at $\beta = 0.03$. Similarly, for the location at the edge of the passage

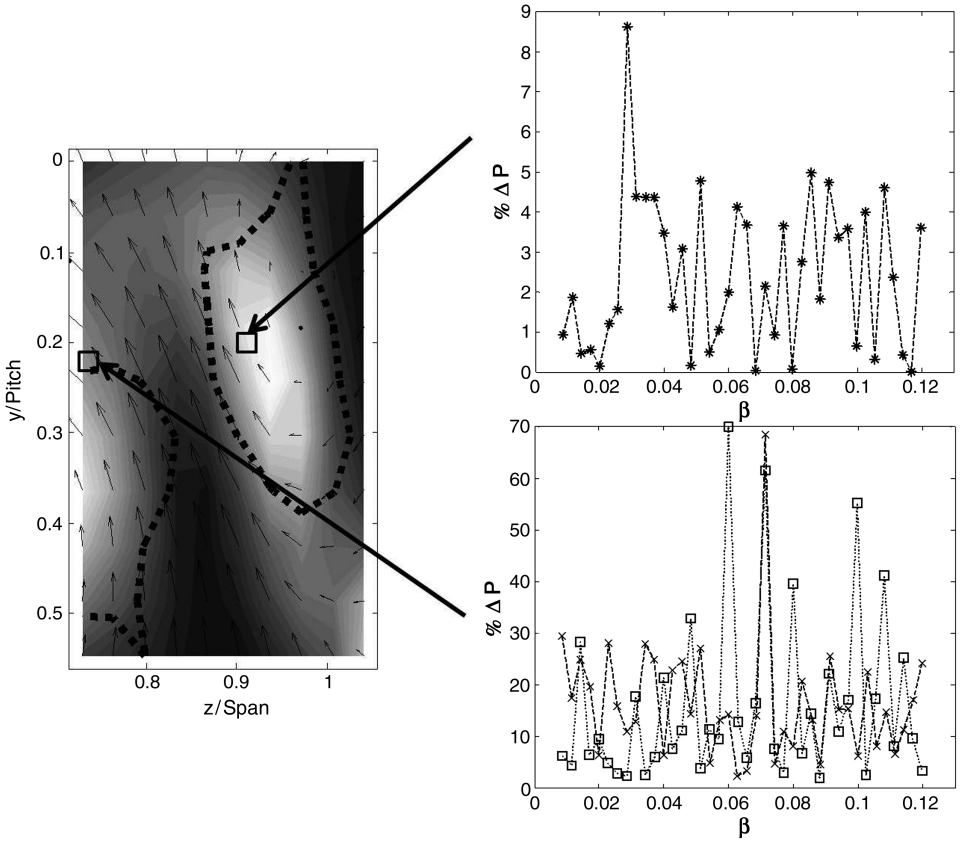

Fig. 7 Effect of varying excitation frequency on downstream total pressure at two specified spacial locations in the wake of the blade row at $Re = 0.5 \times 10^6$.

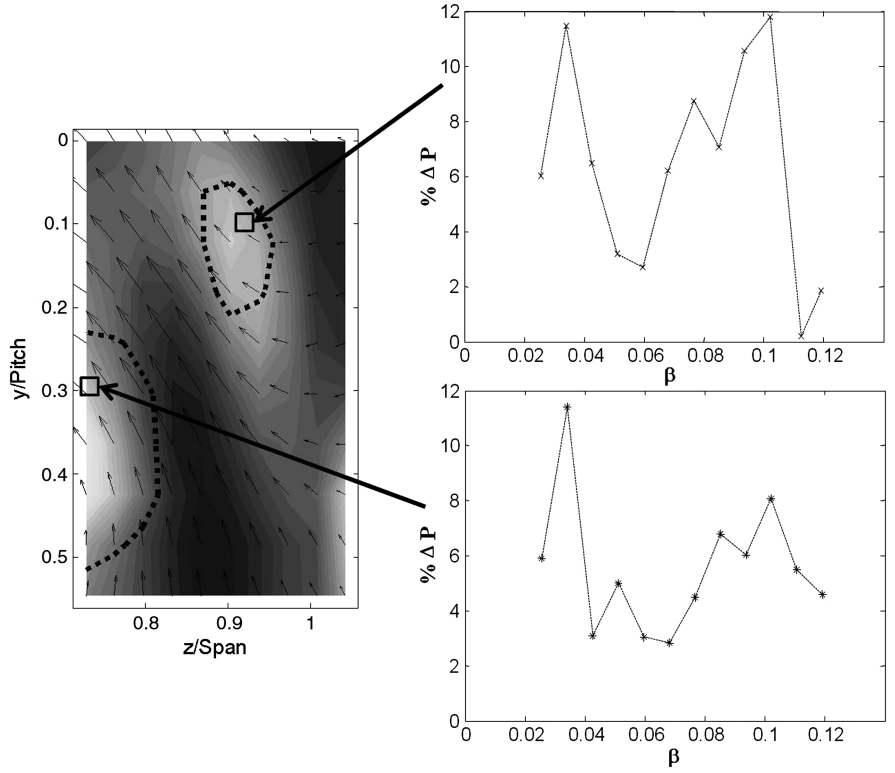

Fig. 8 Effect of varying excitation frequency on downstream total pressure at a specified spacial location in the wake of the blade row at $Re = 0.2 \times 10^6$.

vortex, there is a broad peak between $0.07 \leq \beta \leq 0.1$. Thus, in both cases, the constant Strouhal number for the two cascade velocities supports the notion that the unsteady plasma actuator is exciting an instability in the tip-gap flow region.

Contours of the pressure loss coefficient obtained at $Re_c = 0.2 \times 10^6$ are shown in Fig. 9. A baseline (plasma actuator off) case is shown on the left side of the figure. The other contour plots correspond to plasma actuators operating at different unsteady frequencies. The Strouhal number β is shown above each plot. Included in the contour plots are the zero-level λ_2 contours. These effectively mark the locations and sizes of the tip-leakage and passage vortices.

At $\beta = 0.03$, there was a noticeable decrease in the zero-level λ_2 contour associated with the tip-leakage vortex that is consistent with the single point measurements. At $\beta = 0.07$, there appears to be a small increase in the size of the zero-level λ_2 contour associated with the passage vortex.

At the higher Reynolds number, the differences due to the unsteady excitation are harder to quantify. This is shown in Fig. 10, where again the results for the two Strouhal numbers of 0.03 and 0.07 are shown with respect to the baseline (plasma actuator off).

To obtain a quantitative measure of the effect of the unsteady excitation, the pressure loss coefficients inside the zero-level λ_2 contour associated with the tip-leakage vortex were mass averaged to obtain a total mass-averaged pressure loss coefficient C_{P_T}. The values for different Strouhal numbers at the two Reynolds numbers are shown in Figs. 11 and 12. The bars on each point in the plots represent the repeatability of multiple tests. The C_{P_T} values at $\beta = 0$ correspond to the baseline (plasma actuator off) condition.

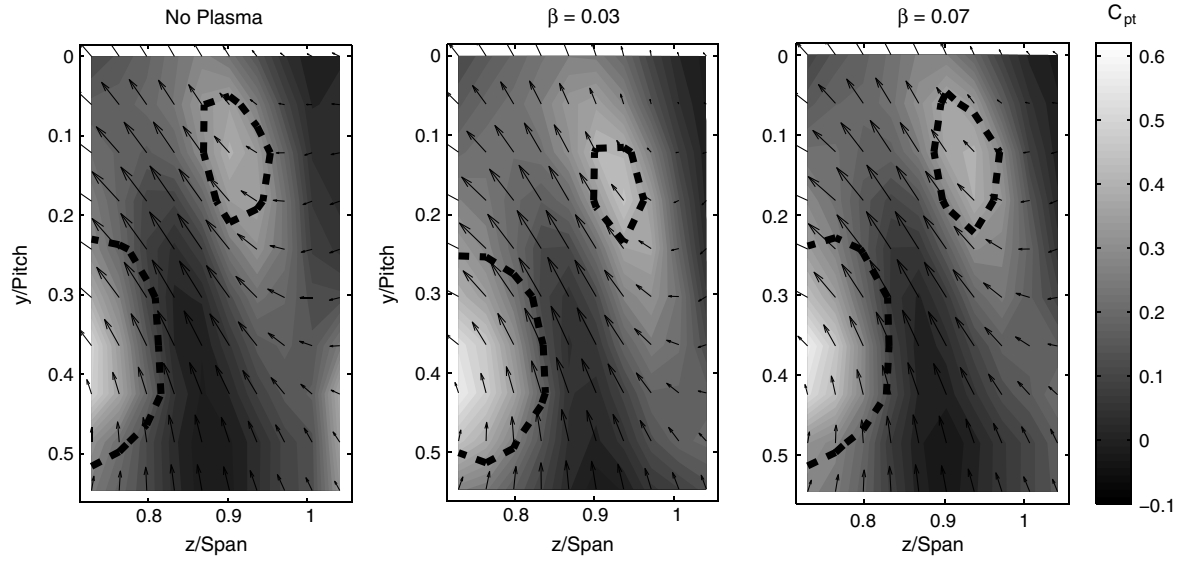

Fig. 9 Pressure loss coefficient contours in the wake, one axial chord downstream of the blade row at a Reynolds number of 0.2×10^6. The color scale is the same for all cases.

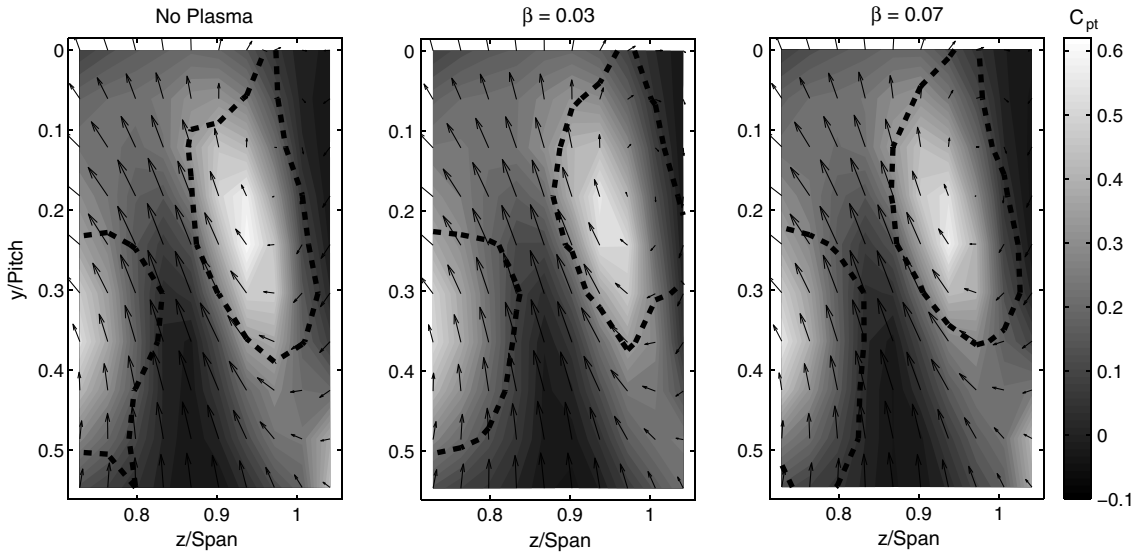

Fig. 10 Pressure loss coefficient contours in the wake, one axial chord downstream of the blade row at a Reynolds number of 0.5×10^6. The color scale is the same for all cases.

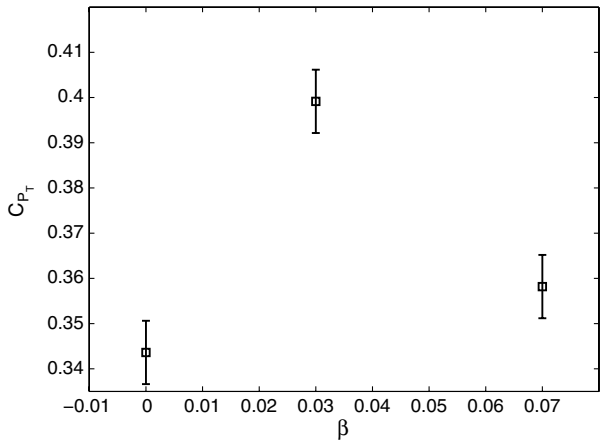

Fig. 11 Mass-averaged total pressure loss coefficients associated with the tip-leakage vortex at a Reynolds number of 0.2×10^6.

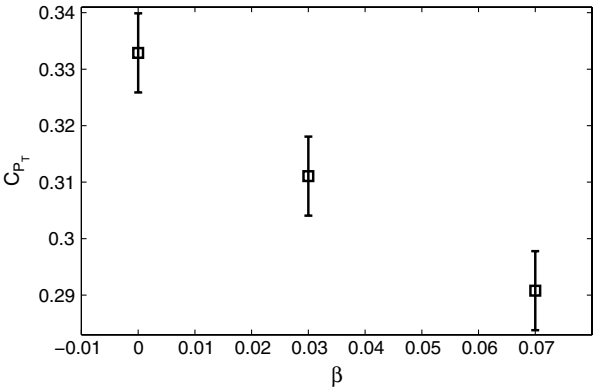

Fig. 12 Mass-averaged total pressure loss coefficients associated with the tip-leakage vortex at a Reynolds number of 0.5×10^6.

At the lower Reynolds number shown in Fig. 11, the mass-averaged pressure loss coefficients increased by 15.0% at $\beta = 0.03$ and 5.6% at $\beta = 0.07$. However, at the higher Reynolds number, shown in Fig. 12, the opposite occurred, with a 6.7% decrease in the C_{P_T} at $\beta = 0.03$ and a 12.6% decrease at $\beta = 0.07$.

It is noted that $\beta = 0.03$ was found to produce the largest change in the pressure loss based on the single point measurements (see Fig. 7). The $\beta = 0.07$ had emerged as a sensitive frequency based on the single point measurements that were located at the edge of the passage vortex. However, based on the mass-averaged loss coefficient, the higher Strouhal number also had an effect on the tip-leakage vortex. The fact that this higher Strouhal number was close to being a harmonic of the lower Strouhal number may be a factor.

The increase in the loss coefficient at the lower Reynolds number could have been the result of having unsteady forcing amplitudes that were too large. The voltage level to the plasma actuator was not

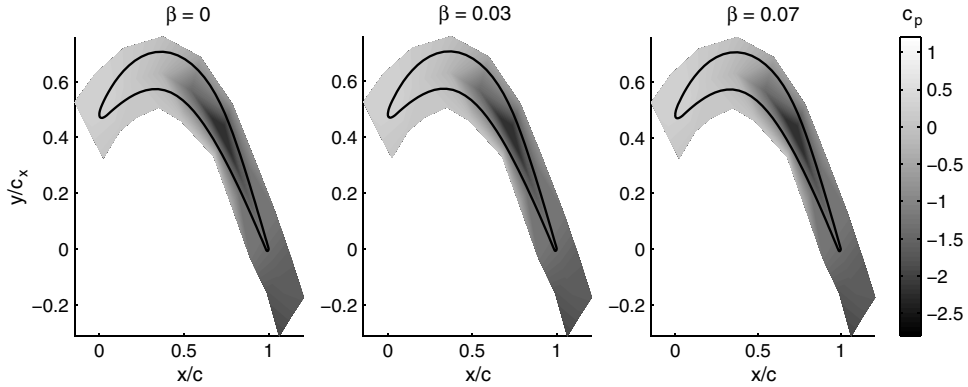

Fig. 13 Endwall static pressure coefficient contours at a gap-to-chord ratio of 4% for two periodic excitation frequencies produced by a plasma actuator on the blade tip.

varied between the two Reynolds numbers in the experiments. Alternatively, the unsteady forcing might have been more amplified at the higher Reynolds number, since instability amplification rates increase with the velocity (Reynolds number). This would have made unsteady excitation more effective at the higher Reynolds number.

As discussed in the Sec. I, the design and operation of the plasma actuator on the blade tip was intended to introduce an unsteady disturbance without increasing the flow blockage through the gap. Evidence that the actuator did not produce any additional flow blockage in the gap is shown by the wall static pressure distributions in Fig. 13. These correspond to $Re_c = 0.5 \times 10^6$. The baseline (plasma actuator off) pressure distribution is denoted as $\beta = 0$. The other two pressure distributions correspond to $\beta = 0.03$ and 0.07 that produced decreases in the mass-averaged loss coefficient. Comparing the three pressure distributions, virtually no difference is observed. This indicates that the plasma actuator did not alter the mean flow passing under the tip gap. Rather than blocking the flow as it comes through the gap, the actuator appears to be working with instabilities inherent in the flow to disrupt the tip-leakage vortex.

VI. Conclusions

A SDBD plasma actuator mounted on the tip of a Pack-B turbine blade in a linear cascade was designed to produce unsteady disturbances that could excite fluid instabilities in the tip-clearance flow. The effect was investigated at inlet Mach numbers of 0.08 and 0.2, corresponding to blade chord Reynolds numbers of 0.2×10^6 and 0.5×10^6. In both cases, a sensitivity of the flow to unsteady forcing was found at nondimensional frequencies of $\beta = 0.03$ and 0.07, based on the tip-gap dimension and the freestream velocity at the cascade inlet.

At the lower Reynolds number, unsteady forcing at the sensitive frequencies resulted in a smaller, stronger tip-leakage vortex. The result was an increase in the mass-averaged total pressure loss coefficient associated with the tip-leakage vortex. Conversely, at the higher Reynolds number, the unsteady forcing produced a reduction in the size and strength of the tip-leakage vortex. The mass-averaged total pressure loss coefficient in this case was reduced by as much as 12.6% for $\beta = 0.07$.

For these, the mean tip-clearance flow, determined by endwall static pressure measurements under the blade, were minimally changed by the unsteady forcing. This indicated that the flow was not restricted from passing under the blade tip. This result indicates that this approach is preferable to passive control strategies, such as squealer tips, that can trap flow under the blade tip in a manner that can lead to excessive blade heating in hot gas flows.

References

[1] Lord, W. K., MacMartin, D. G., and Tillman, T. G., "Flow Control Opportunities in Gas Turbine Engines," AIAA Fluids 2000, Denver, CO, AIAA Paper 2000-2234, 2000.

[2] Yamamoto, A., "Production and Development of Secondary Flows and Losses Within Two Types of Straight Turbine Cascades: Part 1: A Stator Case," *Journal of Turbomachinery*, Vol. 109, No. 2, 1987, pp. 186–193. doi:10.1115/1.3262084

[3] Yamamoto, A., "Production and Development of Secondary Flows and Losses Within Two Types of Straight Turbine Cascades: Part 2: A Rotor Case," *Journal of Turbomachinery*, Vol. 109, No. 2, 1987, pp. 194–200. doi:10.1115/1.3262085

[4] Sjolander, S. A., and Amrud, K. K., "Effects of Tip Clearance on Blade Loading in a Planar Cascade of Turbine Blades," *Journal of Turbomachinery*, Vol. 109, No. 2, 1987, pp. 237–245. doi:10.1115/1.3262090

[5] Yamamoto, A., "Endwall Flow/Loss Mechanisms in a Linear Turbine Cascade With Blade Tip Clearance," *Journal of Turbomachinery*, Vol. 111, No. 3, 1989, pp. 264–275. doi:10.1115/1.3262265

[6] Bindon, J. P., "The Measurement and Formation of Tip Clearance Loss," *Journal of Turbomachinery*, Vol. 111, No. 3, 1989, pp. 257–263. doi:10.1115/1.3262264

[7] Denton, J. D., "Loss Mechanisms in Turbomachines," *Journal of Turbomachinery*, Vol. 115, No. 4, 1993, pp. 621–651. doi:10.1115/1.2929299

[8] Sjolander, S. A., "Secondary and Tip Clearance Flows in Axial Turbines: Physics of Tip-Clearance Flow, I," VKI Lecture Series, Vol. 1, von Kármán Inst. for Fluid Dynamics, Belgium, 1997, pp. 1–32.

[9] McCarter, A. A., "Investigation of Tip Clearance Flow Fields In A Turbine Rotor Passage," M.S. Thesis, Pennsylvania State Univ., University Park, PA, May 2000.

[10] McCarter, A. A., Xiao, X., and Lakshminarayana, B., "Tip Clearance Effects in a Turbine Rotor: Part II: Velocity Field and Flow Physics," *Journal of Turbomachinery*, Vol. 123, No. 2, 2001, pp. 305–313. doi:10.1115/1.1368880

[11] Couch, E., Christophe, J., Hohlfeld, E., and Thole, K. A., "Comparison of Measurements and Predictions for Blowing from a Turbine Blade Tip," *Journal of Propulsion and Power*, Vol. 21, No. 2, 2005, pp. 335–343. doi:10.2514/1.7238

[12] Yamamoto, A., Kondo, Y., and Murao, R., "Cooling-Air Injection Into Secondary Flow and Loss Fields Within a Linear Turbine Cascade," *Journal of Turbomachinery*, Vol. 113, No. 3, 1991, pp. 375–383. doi:10.1115/1.2927886

[13] Dey, D., "Aerodynamic Tip Desensitization in Axial Flow Turbines," Ph.D. Thesis, Pennsylvania State Univ., University Park, PA, 2001.

[14] Douville, T., Stephens, J., Corke, T., and Morris, S., "Turbine Blade Tip Leakage Flow Control by Partial Squealer Tip and Plasma Actuators," 44th Aerospace Sciences Meeting, Reno, NV, AIAA Paper 2006-0020, 2006.

[15] Stephens, J., Corke, T., and Morris, S., "Control of a Turbine Tip Leakage Vortex Using Casing Vortex Generators," 47th Aerospace Sciences Meeting, Orlando, FL, AIAA, 2009-0299, 2009.

[16] Van Ness, D., Corke, T., and Morris, S., "Tip Clearance Flow Visualization of a Turbine Blade Cascade With Active And Passive Control," *Proceedings of ASME Turbo Expo 2008: Power for Land, Sea and Air*, Berlin, American Soc. of Mechanical Engineers, Fairfield, NJ 2008, pp. 1217–1229.

[17] Van Ness, D., Corke, T., and Morris, S., "Tip Clearance Flow Control in a Linear Turbine Cascade Using Plasma Actuation," 47th Aerospace Sciences Meeting, Orlando, FL, AIAA, 2009-0300, 2009.

[18] Bindon, J. P., and Morphis, G., "The Development of Axial Turbine Leakage Loss for Two Profiled Tip Geometries Using Linear Cascade Data," *Journal of Turbomachinery*, Vol. 114, No. 1, 1992, pp. 198–203. doi:10.1115/1.2927985

[19] Ameri, A., and Bunker, R., "Heat Transfer and Flow on the First Stage Blade Tip of a Power Generation Gas Turbine; Part 2: Simulation Results," NASA CR 1999-209151, 1999.

[20] Heyes, F. G., Hodson, H. P., and Dailey, G. M., "The Effect of Blade Tip Geometry on the Tip Leakage Flow in Axial Turbine Cascades," *Journal of Turbomachinery*, Vol. 114, No. 3, 1992, pp. 643–651. doi:10.1115/1.2929188

[21] Key, N. L., and Arts, T., "Comparison of Turbine Tip Leakage Flow For Flat Tip and Squealer Tip Geometries at High-Speed Conditions," *Proceedings of ASME Turbo Expo*, Vienna, Austria, American Soc. of Mechanical Engineers, Fairfield, NJ, 2004, pp. 241–249.

[22] Douville, T. C., "The Effect of Gap Size and Reynolds Number on Turbine Blade Flat and Suction-side Squealer Tip Flowfields," M.S. Thesis, Univ. of Notre Dame, Notre Dame, IN, Dec. 2005.

[23] Bae, J., Breuer, K., and Tan, C., "Control of Tip Clearance Flows in Axial Compressors," AIAA Fluids 2000 Conference and Exhibit, Denver, CO, AIAA, 2000-2233, 2000.

[24] Enloe, C. L., McLaughlin, T. E., Van Dynken, R. D., Kachner, K. D., Jumper, E. J., and Corke, T. C., "Mechanisms and Responses of a Single Dielectric Barrier Plasma Actuator: Plasma Morphology," *AIAA Journal*, Vol. 42, No. 3, 2004, pp. 589–594. doi:10.2514/1.2305

[25] Enloe, C. L., McLaughlin, T. E., Van Dynken, R. D., Kachner, K. D., Jumper, E. J., and Corke, T. C., "Mechanisms and Responses of a Single Dielectric Barrier Plasma Actuator: Geometric Effects," *AIAA Journal*, Vol. 42, No. 3, 2004, pp. 595–604. doi:10.2514/1.3884

[26] Corke, T. C., Post, M. L., and Orlov, D. M., "Single Dielectric Barrier Discharge Plasma Enhanced Aerodynamics: Physics, Modeling and Applications," *Experiments in Fluids*, Vol. 46, No. 1, 2009, pp. 1–26. doi:10.1007/s00348-008-0582-5

[27] Corke, T., Enloe, L., and Wilkinson, S., "Dielectric Barrier Discharge Plasma Actuators for Flow Control," *Annual Review of Fluid Mechanics*, Vol. 42, No. 1, 2010, pp. 505–530. doi:10.1146/annurev-fluid-121108-145550

[28] Post, M., and Corke, T., "Separation Control on High Angle of Attack Airfoil Using Plasma Actuators," *AIAA Journal*, Vol. 42, No. 11, 2004, pp. 2177–2184. doi:10.2514/1.2929

[29] Huang, J., "Documentation and Control of Flow Separation on a Linear Cascade of Pack-B Blades Using Plasma Actuators," Ph.D. Thesis, Univ. of Notre Dame, Notre Dame, IN, 2005.
[30] Huang, J., Corke, T., and Thomas, F., "Plasma Actuators for Separation Control of Low Pressure Turbine Blades," *AIAA Journal*, Vol. 44, No. 1, 2006, pp. 51–57. doi:10.2514/1.2903
[31] Huang, J., Corke, T., and Thomas, F., "Unsteady Plasma Actuators for Separation Control of Low-Pressure Turbine Blades," *AIAA Journal*, Vol. 44, No. 7, 2006, pp. 1477–1487. doi:10.2514/1.19243
[32] Bryer, D. W., and Pankhurst, R., *Pressure Probe Methods for Determining Wind Speed and Flow Direction*, Her Majesty's Stationery Office, London, 1971, pp. 66–74.
[33] Stephens, J., "Control of the Tip-Gap Flow of a Low Pressure Turbine Blade in a Linear Cascade," Ph.D. Dissertation, Univ. of Notre Dame, Notre Dame, IN, April 2009.
[34] Jeong, J., and Hussain, F., "On the Identification of a Vortex," *Journal of Fluid Mechanics*, Vol. 285, 1995, p. 69–94. doi:10.1017/S0022112095000462
[35] Corke, T. C., Post, M. L., and Orlov, D. M., "SDBD Plasma Enhanced Aerodynamics: Concepts, Optimization and Applications," *Progress in Aerospace Sciences*, Vol. 43, Nos. 7–-8, 2007, pp. 193–217. doi:10.1016/j.paerosci.2007.06.001
[36] Ho, C., and Huerre, P., "Perturbed Free Shear Layers," *Annual Review of Fluid Mechanics*, Vol. 16, No. 1, 1984, pp. 365–422. doi:10.1146/annurev.fl.16.010184.002053

R. Miller
Associate Editor